Shifts from a distant neighboring resonance for a four-level atom

M. Horbatsch and E. A. Hessels*

Department of Physics and Astronomy, York University, Toronto, Ontario M3J 1P3, Canada

(Received 15 July 2011; published 16 September 2011)

In a recent paper [Phys. Rev. A **82**, 052519 (2010)], the systematic shifts of a resonance due to quantum-mechanical interference from a distant neighboring resonance were derived. In that paper, the simplest three-level closed system was used to calculate analytic expressions for shifts in the resonant line centers. Here, we extend the analysis to the more relevant four-level system, which consists of two ground states and two excited states and which incorporates the physics of dark states. The shifts are shown to depend on the type of experiment performed and can be much larger than the shifts for the three-level system. The analytic formulas obtained are applied to the $2\,^3S$-to-$2\,^3P$ transitions in atomic helium, where significant shifts are found.

DOI: 10.1103/PhysRevA.84.032508 PACS number(s): 32.70.Jz, 32.80.−t

I. INTRODUCTION

Interference effects from spontaneous radiation from neighboring atomic levels are predicted on the basis of density-matrix equations [1,2] that have been derived from quantum electrodynamics. A range of phenomena results from this interference (most notably quantum beats [3,4]), and a recent measurement shows a clear indication of quantum-mechanical interference for the closely spaced hyperfine components of the D_2 lines of lithium [5]. In a previous paper [6], we presented analytic line shapes for a three-level atom exposed to a monochromatic perturbation and showed that there were shifts that resulted from quantum-mechanical interference between an observed resonance even when the neighboring resonance was distant from the resonance being measured. Reference [6], although useful for illustrating the effect of distant neighboring resonances, presented results that were not immediately applicable to line shifts for viable precision atomic measurements. In the present paper, we extend the calculation to systems that are not closed by allowing for more than one ground state. The line shape for a four-level system is presented in Sec. II. These line shapes reduce to simple approximations when no neighboring resonance is present, as discussed in Sec. III. In Sec. IV, the shifts due to a distant neighboring resonance are presented, and in Sec. V, the derived shifts are applied to the atomic helium $2\,^3S$-to-$2\,^3P$ transitions.

II. FOUR-LEVEL ATOM

We consider a four-level atom with two ground states and two excited states, as shown in Fig. 1. A monochromatic interaction $V(t) = V_0 \cos(\omega t + \phi)$ couples a ground state $|1\rangle$ to two excited states ($|2\rangle$ and $|3\rangle$). In the electric dipole approximation, $V_0 = e\vec{E}_0 \cdot \vec{r}$ for an applied field $\vec{E} = \vec{E}_0 \cos(\omega t + \phi)$. Here, we consider the case where $V(t)$ is nearly resonant with the $|1\rangle \rightarrow |2\rangle$ transition ($\omega = \omega_{21} + \Delta_2$, with $\Delta_2 \ll \omega_{32}$, as illustrated in Fig. 1). We use the rotating-wave approximation, in which the nonresonant $\exp(-i\omega t - i\phi)$ part of $\cos(\omega t + \phi)$ is ignored.

As shown in Fig. 1, both excited states have rates for radiative decay down to the $|1\rangle$ and $|0\rangle$ ground states. Since $V(t)$ does not couple state $|0\rangle$ to any of the other states, it is a dark state, and any population that decays to $|0\rangle$ will remain in this state.

The density-matrix equations for this system are [1,2]

$$\dot{\rho}_{11} = \frac{i\Omega_2}{2}\rho_{12} - \frac{i\Omega_2^*}{2}\rho_{21} + \gamma_{2\rightarrow1}\rho_{22} + \frac{i\Omega_3}{2}\rho_{13} - \frac{i\Omega_3^*}{2}\rho_{31} + \gamma_{23\rightarrow1}(\rho_{23} + \rho_{32}) + \gamma_{3\rightarrow1}\rho_{33}, \tag{1a}$$

$$\dot{\rho}_{12} = \frac{i\Omega_2^*}{2}(\rho_{11} - \rho_{22}) - \left(\frac{\gamma_2}{2} + i\Delta_2\right)\rho_{12} - \frac{\gamma_{23}}{2}\rho_{13} - \frac{i\Omega_3^*}{2}\rho_{32}, \tag{1b}$$

$$\dot{\rho}_{22} = \frac{i\Omega_2^*}{2}\rho_{21} - \frac{i\Omega_2}{2}\rho_{12} - \gamma_2\rho_{22} - \frac{\gamma_{23}}{2}(\rho_{23} + \rho_{32}), \tag{1c}$$

$$\dot{\rho}_{13} = \frac{i\Omega_3^*}{2}(\rho_{11} - \rho_{33}) - \frac{\gamma_{23}}{2}\rho_{12} - \frac{i\Omega_2^*}{2}\rho_{23} - \left[\frac{\gamma_3}{2} + i(\Delta_2 - \omega_{32})\right]\rho_{13}, \tag{1d}$$

$$\dot{\rho}_{23} = \frac{i\Omega_3^*}{2}\rho_{21} - \frac{\gamma_{23}}{2}(\rho_{22} + \rho_{33}) - \frac{i\Omega_2}{2}\rho_{13} - \left(\frac{\gamma_2 + \gamma_3}{2} - i\omega_{32}\right)\rho_{23}, \tag{1e}$$

$$\dot{\rho}_{33} = \frac{i\Omega_3^*}{2}\rho_{31} - \frac{i\Omega_3}{2}\rho_{13} - \gamma_3\rho_{33} - \frac{\gamma_{23}}{2}(\rho_{23} + \rho_{32}), \tag{1f}$$

where $\Omega_2 = \langle 1|V_0 e^{i\phi}|2\rangle/\hbar$ and $\Omega_3 = \langle 1|V_0 e^{i\phi}|3\rangle/\hbar$ are Rabi frequencies, Ω_2^* and Ω_3^* are their complex conjugates, $\hbar\Delta_2 = \hbar(\omega - \omega_{21})$ and $\hbar\omega_{32}$ are the energy differences shown in Fig. 1, and $\tau_2 = \gamma_2^{-1}$ and $\tau_3 = \gamma_3^{-1}$ are the lifetimes of states $|2\rangle$ and $|3\rangle$. In terms of the partial decay rates shown in Fig. 1, $\gamma_2 = \gamma_{2\rightarrow1} + \gamma_{2\rightarrow0}$, $\gamma_3 = \gamma_{3\rightarrow1} + \gamma_{3\rightarrow0}$, and $\gamma_{23} = \gamma_{23\rightarrow1} + \gamma_{23\rightarrow0}$, where (in the electric dipole approximation)

$$\gamma_{i\rightarrow j} = \frac{4e^2|\omega_{ji}|^3}{3\hbar c^3}\langle i|\vec{r}|j\rangle \cdot \langle j|\vec{r}|i\rangle, \tag{2a}$$

and

$$\gamma_{23\rightarrow j} = \frac{4e^2|\omega_{j2}|^3}{3\hbar c^3}\langle 2|\vec{r}|j\rangle \cdot \langle j|\vec{r}|3\rangle. \tag{2b}$$

Here, we have assumed $\omega_{32} \ll \omega_{21}, \omega_{20}$. The inclusion of the $\gamma_{23\rightarrow j}$ terms in Eq. (1) results directly from quantum-mechanical interference of the radiative decay.

*hessels@yorku.ca

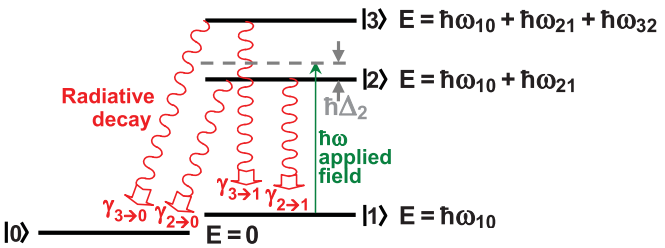

FIG. 1. (Color online) The four-level system considered in this paper. A single field of angular frequency ω couples $|1\rangle$ to $|2\rangle$ and to $|3\rangle$, both of which can decay to $|0\rangle$ and $|1\rangle$. We consider the case in which the field is nearly in resonance with the $|1\rangle \rightarrow |2\rangle$ transition and study the shifts in this resonance due to the distant $|1\rangle \rightarrow |3\rangle$ resonance. The figure shows state $|3\rangle$ above state $|2\rangle$ (i.e., $\omega_{32} > 0$), but the results derived also apply for the case when state $|3\rangle$ is below state $|2\rangle$ (i.e., $\omega_{32} < 0$).

Equation (1), along with the complex-conjugate equations for $\dot{\rho}_{21}$, $\dot{\rho}_{32}$, and $\dot{\rho}_{31}$, can be used to obtain ρ_{11}, ρ_{22}, and ρ_{33}, the populations of states $|1\rangle$, $|2\rangle$, and $|3\rangle$, while ρ_{00} then can be obtained from $\rho_{00} + \rho_{11} + \rho_{22} + \rho_{33} = 1$. The equations for $\dot{\rho}_{01}$, $\dot{\rho}_{10}$, $\dot{\rho}_{02}$, $\dot{\rho}_{03}$, and $\dot{\rho}_{30}$ are not needed, since ρ_{01}, ρ_{10}, ρ_{02}, ρ_{20}, ρ_{03}, and ρ_{30} do not appear on the right-hand side of Eq. (1) and, therefore, are decoupled from these differential equations.

For this paper, we consider the case where the population starts in state $|1\rangle$ and the $|1\rangle \rightarrow |3\rangle$ transition is sufficiently out of resonance so that, after interacting with $V(t)$ for a time T, very little population is excited to state $|3\rangle$. We introduce a small ordering parameter η, and in terms of this parameter, the population of $|3\rangle$ is η^2 times smaller than the population of the other states. For this to occur, it is necessary that Δ_2, Ω_2, Ω_3, $\gamma_{2\rightarrow1}$, $\gamma_{2\rightarrow0}$, $\gamma_{3\rightarrow1}$, $\gamma_{3\rightarrow0}$, and $2\pi/T$ all be smaller (by 1 order of η) than ω_{32}. The density-matrix elements ρ_{13}, ρ_{31}, ρ_{23}, and ρ_{32} will also be an order of η smaller than the dominant elements: ρ_{11}, ρ_{12}, ρ_{21}, and ρ_{22}.

Taking linear combinations of Eqs. (1a)–(1e) (and their complex conjugates), allows one to eliminate (to order η) the ρ_{13}, ρ_{31}, ρ_{23}, and ρ_{32} terms in Eqs. (1a)–(1c), yielding differential equations that include all corrections up to first order in η,

$$\dot{\rho}_{11} = \frac{i\Omega_2''}{2}\rho_{12} - \frac{i\Omega_2''^*}{2}\rho_{21} + \gamma_{2\rightarrow1}\rho_{22}, \tag{3a}$$

$$\dot{\rho}_{12} = \frac{i\Omega_{2+}'^*}{2}\rho_{11} - \left(\frac{\gamma_2}{2} + i\Delta_2'\right)\rho_{12} - \frac{i\Omega_{2-}'^*}{2}\rho_{22}, \tag{3b}$$

$$\dot{\rho}_{22} = \frac{i\Omega_{2+}'^*}{2}\rho_{21} - \frac{i\Omega_{2+}'}{2}\rho_{12} - \gamma_2\rho_{22}, \tag{3c}$$

where the order η corrections come from $\Omega_{2\pm}' = \Omega_2 \pm i\frac{1}{2}\gamma_{23}\Omega_3/\omega_{32}$, $\Omega_2'' = \Omega_2 - i\frac{1}{2}(\gamma_{23} - 2\gamma_{23\rightarrow1})\Omega_3/\omega_{32}$, and from

$$\Delta_2' = \Delta_2 - \frac{\gamma_{23}^2 + |\Omega_3|^2}{4\omega_{32}}. \tag{4}$$

Combining Eqs. (3a)–(3c) leads to a fourth-order differential equation that describes ρ_{11} and ρ_{22} up to first order in η,

$$\begin{aligned} 4\frac{d^4\rho_{ii}}{dt^4} + 8\gamma_2\frac{d^3\rho_{ii}}{dt^3} + \left(5\gamma_2^2 + 4\Delta_2'^2 + 4|\Omega_2|^2\right)\frac{d^2\rho_{ii}}{dt^2} \\ + \left[\gamma_2^3 + 4\gamma_2\Delta_2'^2 + 2(2\gamma_2 - \gamma_{2\rightarrow1}')|\Omega_2|^2\right]\frac{d\rho_{ii}}{dt} \\ + (2\gamma_2 - \gamma_2' - 2\gamma_{2\rightarrow1}' + \gamma_{2\rightarrow1})\gamma_2|\Omega_2|^2\rho_{ii} = 0, \end{aligned} \tag{5}$$

where

$$\gamma_{2\rightarrow1}' = \gamma_{2\rightarrow1} - \gamma_{23\rightarrow1}\frac{\Delta_2\Omega_3}{\omega_{32}\Omega_2}, \tag{6a}$$

$$\gamma_2' = \gamma_2 + 2\gamma_{23}\frac{\Delta_2\Omega_3}{\omega_{32}\Omega_2}. \tag{6b}$$

For an atom that starts in state $|1\rangle$ at $t = 0$, the solution to Eq. (5) at time $t = T$ is

$$\rho_{ii} = \sum_{s,\sigma}^{\pm1} \frac{\sigma s C_{s\sigma}^{(ii)} v e^{-\lambda_{s\sigma}T/2}}{4R_s(2sv^3 - 2\sigma v^2 R_s + \gamma_{2\rightarrow1}'|\Omega_2|^2)}, \tag{7}$$

where

$$\lambda_{s\sigma} = \gamma_2 - sv + \sigma R_s, \tag{8a}$$

$$R_s = s\sqrt{\frac{2p}{u} - 2u - 2\alpha + s\frac{\gamma_{2\rightarrow1}'|\Omega_2|^2}{v}}, \tag{8b}$$

$$v = \sqrt{2u - \alpha - \frac{2p}{u}}, \tag{8c}$$

$$u = \sqrt[3]{q + \sqrt{q^2 + p^3}}, \tag{8d}$$

$$q = \frac{\alpha^3}{64} + \frac{\alpha\gamma_2^2\Delta_2''^2}{16} + \frac{\gamma_{2\rightarrow1}'^2|\Omega_2|^4}{64}, \tag{8e}$$

$$p = \frac{\gamma_2^2\Delta_2''^2}{12} - \frac{\alpha^2}{16}, \tag{8f}$$

$$\alpha = \frac{2}{3}\left(|\Omega_2|^2 + \Delta_2'^2\right) - \frac{\gamma_2^2}{6}, \tag{8g}$$

$$\begin{aligned} C_{s\sigma}^{(11)} &= \left[R_{-s}^2 - (\gamma_2 + sv)^2\right](\gamma_2 - \sigma R_s - sv) \\ &\quad - 2|\Omega_2|^2(\sigma R_s - sv - 3\gamma_2 + 2\gamma_{2\rightarrow1}' + \gamma_2'), \end{aligned} \tag{8h}$$

$$C_{s\sigma}^{(22)} = 2|\Omega_2|^2(\sigma R_s - sv), \tag{8i}$$

with

$$\Delta_2'' = \Delta_2' + \frac{|\Omega_2|^2\Omega_3(2\gamma_{23} - \gamma_{23\rightarrow1})}{2\Omega_2\omega_{32}\gamma_2}. \tag{9}$$

Equations (7) and (8) are the solutions to Eqs. (1a)–(1f) for ρ_{11} and ρ_{22} up to first order in η. Up to this order, $\rho_{33} = 0$ and $\rho_{00} = 1 - \rho_{11} - \rho_{22}$. The presence of state $|3\rangle$ appears in this solution only through the primed quantities (γ_2', $\gamma_{2\rightarrow1}'$, Δ_2', and Δ_2''), and these primed quantities lead to perturbations and shifts in the resonant line shapes (as discussed in Sec. IV). First, in Sec. III, we investigate the line shape in the absence of perturbations due to state $|3\rangle$.

III. THREE-LEVEL ATOM

In the limit of $\omega_{32} \rightarrow \infty$ (which is equivalent to $\eta \rightarrow 0$ or to the absence of perturbations from state $|3\rangle$), the primed

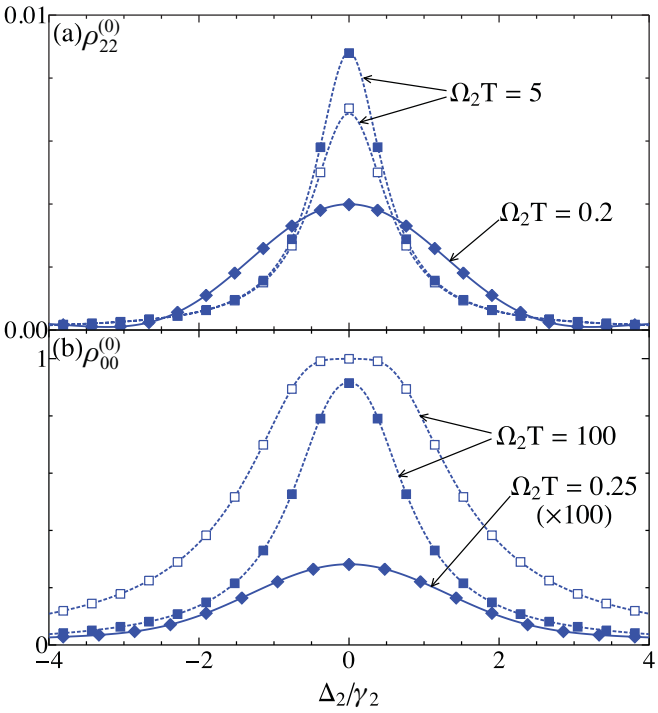

FIG. 2. (Color online) Line shapes for the three-level system, with the $|2\rangle$ and $|0\rangle$ state populations as a function of applied frequency $\omega = \omega_{21} + \Delta_2$ shown in (a) and (b), respectively. These line shapes Eq. (7) are for $\Omega_2 = 0.1\gamma_2$ with $\gamma_{2\to1}/\gamma_2 = 0.25$ (closed symbols) and 0.75 (open symbols). The solid lines are the approximate line shapes of Eqs. (10) and (11), which show good agreement at small $\Omega_2 T$. The dotted lines are the approximate line shapes of Eqs. (14) and (15), which show good agreement with Eq. (7) at larger $\Omega_2 T$.

quantities in Eq. (8) approach their unprimed values ($\gamma_2' \to \gamma_2$, $\gamma_{2\to1}' \to \gamma_{2\to1}$, and $\Delta_2', \Delta_2'' \to \Delta_2$), and ρ_{ii} approach their unperturbed expressions $\rho_{ii}^{(0)}$. The unperturbed $\rho_{00}^{(0)}$, $\rho_{11}^{(0)}$, and $\rho_{22}^{(0)}$ give the populations of the $|0\rangle$, $|1\rangle$, and $|2\rangle$ states for the simpler three-level system that corresponds to the absence of state $|3\rangle$ in Fig. 1. When plotted against the angular frequency ω of the applied field, the $\rho_{ii}^{(0)}$ give the unperturbed line shapes, examples of which are shown in Fig. 2. Here, $\rho_{11}^{(0)}$ is not considered since it can be obtained from $\rho_{11}^{(0)} = 1 - \rho_{22}^{(0)} - \rho_{00}^{(0)}$.

From inspection of Eq. (8), it can be seen that the $\rho_{ii}^{(0)}$ line shapes depend only on the square of Δ_2 and, therefore, are symmetric about $\Delta_2 = 0$ (thus, their line center is unshifted from $\omega = \omega_{21}$). The widths and amplitudes of these line shapes depend on the time T that the monochromatic $V(t)$ is applied, the Rabi frequency (Ω_2), and the decay rates γ_2 and $\gamma_{2\to1}$, as illustrated in Fig. 3. Since the population is assumed to start in state $|1\rangle$, $\rho_{22}^{(0)} = 0$ and $\rho_{00}^{(0)} = 0$ at $T = 0$, but all of the population goes into the dark state ($\rho_{00}^{(0)} = 1$ and $\rho_{22}^{(0)} = 0$) in the limit of large T, as shown in Figs. 3(a) and 3(b). The widths of the line shapes are approximately the natural width for a π pulse ($\Omega_2 T = \pi$) and become broader for short times T and for large $\Omega_2 T$, as shown in Figs. 3(c) and 3(d).

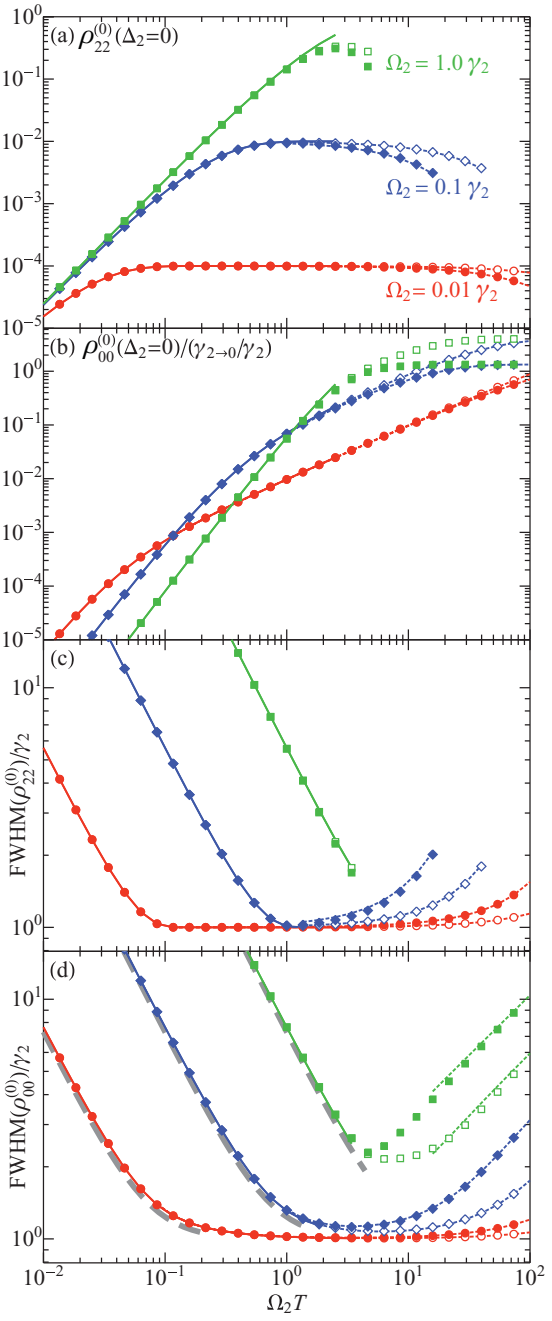

FIG. 3. (Color online) Amplitudes and widths for the three-level line shapes for $\Omega_2/\gamma_2 = 1$ (squares), 1/10 (diamonds), and 1/100 (circles) for a range of $\Omega_2 T$. The on-resonance amplitudes are shown in (a) and (b) for the $|2\rangle$ and $|0\rangle$ state populations. The full width at half maximum (FWHM) is shown in parts (c) and (d). For small $\Omega_2 T$, the widths and amplitudes agree with Eqs. (10) and (11), which are represented by the solid lines. For larger $\Omega_2 T$, they agree with Eqs. (14) and (15), shown here as dotted lines. The plots show both $\gamma_{2\to1}/\gamma_2 = 0.25$ (closed symbols) and 0.75 (open symbols), but it is only for larger $\Omega_2 T$ that the line shapes depend on this branching ratio, as shown by the bifurcated curves at the right of the plots. Data points and curves are discontinued at the right when the line shapes are no longer simple peaks. The heavy dashed lines in (d) show that, for small $\Omega_2 T$, the width of the $|0\rangle$ state is approximated well by adding the natural width in quadrature with the width of Eq. (13).

For the case of small $\Omega_2 T$, the line shapes [Eq. (7), with $\omega_{32} \to \infty$] become

$$\rho_{22}^{(0)} \approx |\Omega_2|^2 \frac{1 + e^{-\gamma_2 T} - 2\cos[\Delta_2 T] e^{-\gamma_2 T/2}}{4\Delta_2^2 + \gamma_2^2}, \quad (10)$$

and

$$\rho_{00}^{(0)} \approx \frac{\gamma_{2\to 0}}{\gamma_2^2 + 4\Delta_2^2} |\Omega_2|^2 \left[T + \frac{1 - e^{-\gamma_2 T}}{\gamma_2} - 4e^{-\gamma_2 T/2} \frac{\gamma_2 e^{\gamma_2 T/2} - \gamma_2 \cos(\Delta_2 T) + 2\Delta_2 \sin(\Delta_2 T)}{\gamma_2^2 + 4\Delta_2^2} \right]. \quad (11)$$

The amplitudes and widths of these line shapes are shown as solid lines in Fig. 2 and on the left-hand portions of Fig. 3, where it can be seen that they agree well with the data points [from the full line shape of Eq. (7)]. For small T ($T \ll \gamma_2^{-1}, \gamma_{2\to 1}^{-1}, \Omega_2^{-1}$), Eqs. (10) and (11) further reduce to the familiar,

$$\rho_{22}^{(0)} \approx |\Omega_2|^2 \frac{\sin^2(\Delta_2 T/2)}{\Delta_2^2}, \quad (12)$$

and the less familiar,

$$\rho_{00}^{(0)} \approx \frac{\gamma_{2\to 0}}{2\Delta_2^3} |\Omega_2|^2 [\Delta_2 T - \sin(\Delta_2 T)]. \quad (13)$$

On the other hand, for large $\gamma_2 T$ and not too large values of $\Omega_2 T$, the line shapes [Eq. (7), with $\omega_{32} \to \infty$] reduce to

$$\rho_{22}^{(0)} \approx \frac{|\Omega_2|^2}{\gamma_2^2 + 4\Delta_2^2} \exp\left[-\frac{\gamma_{2\to 0}}{\gamma_2^2 + 4\Delta_2^2} |\Omega_2|^2 T \right], \quad (14)$$

and

$$\rho_{00}^{(0)} \approx 1 - \left[1 + \frac{\gamma_{2\to 0}}{\gamma_2} |\Omega_2|^2 \frac{3\gamma_2^2 - 4\Delta_2^2}{(\gamma_2^2 + 4\Delta_2^2)^2} \right] \times \exp\left[-\frac{\gamma_{2\to 0}}{\gamma_2^2 + 4\Delta_2^2} |\Omega_2|^2 T \right], \quad (15)$$

as indicated by the dotted lines in Figs. 2 and 3, which show that these approximations work well for larger $\Omega_2 T$. The solid and dotted lines in Fig. 3 show that the combination of Eqs. (10), (11), (14), and (15) is sufficient for approximating the full line shapes for most of the useful parameter space, reducing the need for using the more complicated full line shapes of Eq. (7).

IV. SHIFTS

The line shapes of Sec. III are perturbed when state $|3\rangle$ is included. The perturbations are small if η is small (ω_{32} is large), but, even in this case, the resulting shifts in the line centers can be important for precision measurements. Up to first order in η, the modified line shapes are given exactly by Eqs. (7) and (8). In the limit of small $\Omega_2 T$, the line shapes can be approximated by

$$\rho_{22} \approx |\Omega_2|^2 \frac{1 + e^{-\gamma_2 T} - 2\cos[\Delta_2' T] e^{-\gamma_2 T/2}}{4\Delta_2'^2 + \gamma_2^2}, \quad (16)$$

and

$$\rho_{00} \approx \frac{|\Omega_2|^2}{\gamma_2^2 + 4\Delta_2'^2} \left\{ (\gamma_{2\to 0} - 2\xi\Delta_2) \left[T + \frac{1 - e^{-\gamma_2 T}}{\gamma_2} - 4e^{-\gamma_2 T/2} \frac{\gamma_2 e^{\gamma_2 T/2} - \gamma_2 \cos(\Delta_2' T) + 2\Delta_2' \sin(\Delta_2' T)}{\gamma_2^2 + 4\Delta_2'^2} \right] + 2\xi\Delta_2 \frac{1 - e^{-\gamma_2 T}}{\gamma_2} - 2\xi\Delta_2 e^{-\gamma_2 T/2} \frac{\sin(\Delta_2' T)}{\Delta_2'} \right\}, \quad (17)$$

where

$$\xi = \frac{\Omega_3 \gamma_{23\to 0}}{\Omega_2 \omega_{32}}. \quad (18)$$

Equations (16) and (17) are generalizations of Eqs. (10) and (11), respectively. For small T ($T \ll \gamma_2^{-1}, \gamma_{2\to 1}^{-1}, \Omega_2^{-1}$), they reduce to

$$\rho_{22} \approx |\Omega_2|^2 \frac{\sin^2(\Delta_2' T/2)}{\Delta_2'^2}, \quad (19)$$

and

$$\rho_{00} \approx \frac{\gamma_{2\to 0} - 2\xi\Delta_2}{2\Delta_2'^3} |\Omega_2|^2 [\Delta_2' T - \sin(\Delta_2' T)]. \quad (20)$$

Equation (16) differs from Eq. (10) only by the replacement of Δ_2 by Δ_2'. Similarly, Eq. (19) differs from Eq. (12) by the replacement of Δ_2 by Δ_2'. Therefore, in both limits, the ρ_{22} line shape is shifted from $\omega = \omega_{21}$ by

$$Sh^{(22)} \approx \mathcal{S}_0 = \frac{\gamma_{23}^2 + |\Omega_3|^2}{4\omega_{32}}. \quad (21)$$

In both cases, other than this shift, the line shapes are identical to the unperturbed line shapes.

Equations (17) and (20), however, are also shifted due to the presence of ξ [Eq. (18)] in these equations. The ξ-dependent terms cause both shifts and line-shape distortions. The shifts can be estimated by evaluating these terms at the half-maximum points and dividing by the slope at the half-maximum points. We note that the line shape of Eq. (13) has a FWHM of $2.3\pi/T$ and the width of Eq. (11) is approximated by this added in quadrature with the natural width (γ_2), as shown by the heavy dashed line in Fig. 3(d).

Using this approximation, the total shift of the ρ_{00} line shape of Eq. (20) (due to a combination of the effect of Δ_2' and of ξ) is

$$Sh^{(00)} \approx \mathcal{S}_0 - \frac{9.89}{\gamma_{2\to 0}} \frac{\xi}{T^2}. \quad (22)$$

The shift in Eq. (17) can be approximated by a series expansion,

$$Sh^{(00)} \approx \mathcal{S}_0 - \frac{\xi\gamma_2^2}{\gamma_{2\to 0}} f(\gamma_2 T), \quad (23)$$

with

$$f(\gamma_2 T) \approx \frac{9.89}{(\gamma_2 T)^2} + \frac{2.14}{\gamma_2 T} + 0.164 + 0.0148\gamma_2 T. \quad (24)$$

For larger $\Omega_2 T$, the generalization of Eqs. (14) and (15) to include the perturbation from state $|3\rangle$ gives

$$\rho_{22} \approx \frac{|\Omega_2|^2}{\gamma_2^2 + 4\Delta_2'^2} \exp\left[-\frac{\gamma_{2\to 0} - 2\xi\Delta_2}{\gamma_2^2 + 4\Delta_2'^2} |\Omega_2|^2 T \right], \quad (25)$$

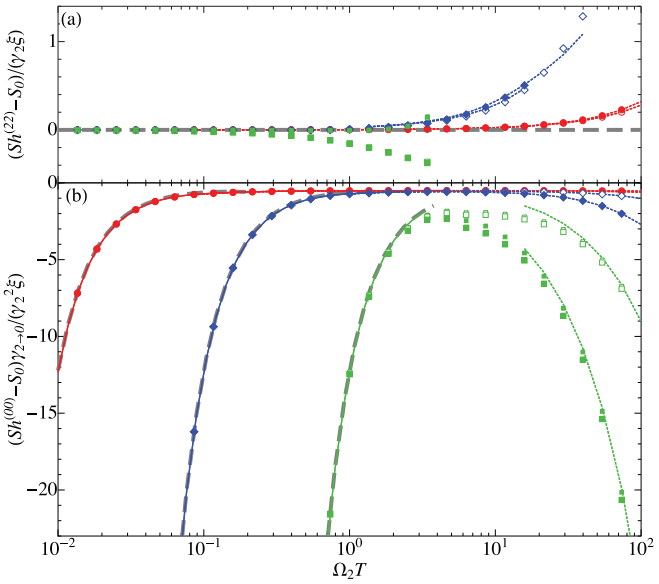

FIG. 4. (Color online) Shifts due to quantum-mechanical interference with the distant $|1\rangle$-to-$|3\rangle$ resonance for $\Omega_2/\gamma_2 = 1$ (squares), 1/10 (diamonds), and 1/100 (circles) for a range of $\Omega_2 T$ for the (a) ρ_{22} line shape and the (b) ρ_{00} line shape. For small $\Omega_2 T$, the shifts agree with Eqs. (16) and (17), which are represented by the solid lines. The heavy dashed line shows the approximations of Eqs. (21) and (23). For larger $\Omega_2 T$, the shifts agree with Eqs. (25) and (26), shown here as dotted lines. The plots show both $\gamma_{2\to1}/\gamma_2 = 0.25$ (closed symbols) and 0.75 (open symbols), but it is only for larger $\Omega_2 T$ that the shifts depend on this branching ratio, as shown by the bifurcated curves at the right of the plots. Additionally, the shifts show a small dependence on $\gamma_{23\to1}/\gamma_{23}$, which can be seen from further bifurcations at the right between $\gamma_{23\to1}/\gamma_{23} = 0.25$ (small plot symbols) and $\gamma_{23\to1}/\gamma_{23} = 0.75$ (large plot symbols). As with Fig. 3, the symbols and plot lines are discontinued to the right when the line shapes are no longer simple peaks.

and

$$\rho_{00} \approx 1 - \left[1 + |\Omega_2|^2 \frac{\gamma_{2\to0}\left(3\gamma_2^2 - 4\Delta_2'^2\right) - 8\xi\,\Delta_2\gamma_2^2}{\gamma_2\left(\gamma_2^2 + 4\Delta_2'^2\right)^2}\right] \times \exp\left[-\frac{\gamma_{2\to0} - 2\xi\,\Delta_2}{\gamma_2^2 + 4\Delta_2'^2}|\Omega_2|^2 T\right]. \quad (26)$$

Both Eqs. (25) and (26) exhibit shifts due to both Δ_2' and ξ.

Figure 4 shows the shifts for the ρ_{22} and ρ_{00} line shapes for the same set of parameters as used in Fig. 3. The shifts in the figure are calculated from Eq. (7), and the lines in the plot show that the approximations developed in this section give good estimates for the shifts. It should be noted that the shifts depend on whether the resonance line center is determined by monitoring the $|2\rangle$ state population [ρ_{22} of Fig. 4(a)] or the $|0\rangle$ state population [ρ_{00} of Fig. 4(b)]. The shifts are especially large if the $|0\rangle$ state population is measured and if $T < \gamma_2^{-1}$ or Ω_2 is large. The shifts shown in Fig. 4 have the $\mathcal{S}_0$ shifts subtracted. In Ref. [6], it was shown that the $\mathcal{S}_0$ shift includes both the ac Stark shift and an additional shift due to quantum-mechanical interference. Reference [6] discusses how this additional shift is of concern for precision measurements for which the precision of the measurement is N times smaller than the natural width if the neighboring resonance (state $|3\rangle$) is within N natural widths of the resonance being measured. Some of the shifts shown in Fig. 4 are much larger than $\mathcal{S}_0$, and thus, even more distant neighboring resonances can be of concern for systems with four or more states.

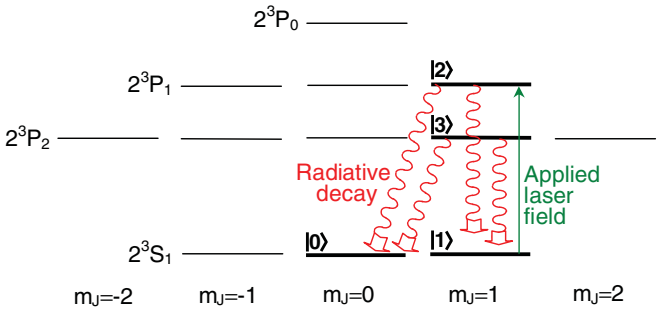

FIG. 5. (Color online) The $n = 2$ triplet states of helium. For atoms prepared in state $|1\rangle$ and a linearly polarized laser (as shown), the states $|0\rangle$–$|3\rangle$, which are shown, form a closed four-level system, such as that of Fig. 1. As in Fig. 1, the applied field is nearly resonant with the $|1\rangle$-to-$|2\rangle$ transition, and interference with the far-off-resonant $|1\rangle$-to-$|3\rangle$ transition causes small shifts. Since in this case, state $|3\rangle$ is below state $|2\rangle$, a negative value of ω_{32} must be used in the equations of Secs. II and IV.

V. THE $n = 2$ TRIPLET STATES OF HELIUM

To illustrate the shifts, we consider the helium $2\,^3S$-to-$2\,^3P$ transitions, as shown in Fig. 5. The $2\,^3S$-to-$2\,^3P$ transitions have been measured precisely in order to determine the Lamb shift for the helium atom [7] and in order to determine the fine-structure constant [8–12].

In order to connect with the derivations in Sec. IV, we assume that the initial population is optically pumped into the $2\,^3S_1$ ($m_J = 1$) state (labeled $|1\rangle$ in Fig. 5) and that this state is coupled by a linearly polarized laser field to the $2\,^3P_1$ ($m_J = 1$) state (labeled $|2\rangle$ in Fig. 5). This laser is also coupled (far-off resonance) with the $2\,^3P_2$ ($m_J = 1$) state (labeled $|3\rangle$ in Fig. 5), and both states $|2\rangle$ and $|3\rangle$ decay radiatively to both state $|1\rangle$ and to the $2\,^3S_1$ ($m_J = 0$) state (labeled $|0\rangle$ in Fig. 5). State $|0\rangle$ is a dark state since its near-resonant coupling to the $2\,^3P_1$ ($m_J = 0$) state is electric dipole forbidden. Thus, states $|0\rangle$–$|3\rangle$ form a closed system, and the shifts derived in the previous sections apply.

For this system, $\omega_{32} = -2\pi$ (2.29 GHz), $\gamma_2^{-1} = \gamma_3^{-1} =$ 98 ns, $\gamma_{2\to0} = \gamma_{2\to1} = \gamma_{3\to0} = \gamma_{3\to1} = \gamma_{23\to1} = \gamma_2/2$, and, because of the equality of the $\langle 1|z|2\rangle$ and $\langle 1|z|3\rangle$ matrix elements, $\Omega_2 = \Omega_3$. However, because $\langle 0|\vec{r}|2\rangle = -\langle 0|\vec{r}|3\rangle$, $\gamma_{23\to0} = -\gamma_2/2$, which results in $\gamma_{23} = 0$. Thus, $\mathcal{S}_0$ is given by only $|\Omega_3|^2/(4\omega_{32})$, which is just the usual ac Stark shift. The additional shifts are all due to the small parameter $\xi = 3.55 \times 10^{-4}$, and these shifts are listed in Table I.

The shifts in Table I are large compared to the 0.30- and 0.35-kHz uncertainties of recent precise measurements in this system [8,9]. Each row in Table I shows the shifts for observing the $|0\rangle$ or $|2\rangle$ state populations after a particular interaction time (T) at three different Rabi frequencies (three different intensities of the applied field). It is clear that the shift is much more pronounced if the $|0\rangle$ state population

TABLE I. Frequency shifts for the helium $2\,^3S$-to-$2\,^3P$ transition shown in Fig. 5. The shifts depend on which population is being monitored as well as on the Rabi frequency Ω_2 and interaction time T as indicated. The shifts shown are in addition to shifts caused by the ac Stark effect given by Eq. (21) and are calculated by evaluating the difference in ρ_{ii} [using Eq. (7)] at the two half-maximum points of $\rho_{ii}^{(0)}$ and dividing by the slope of $\rho_{ii}^{(0)}$ at these points. The listed values are in kiloHertz and represent frequency (not angular frequency) shifts. The values in square brackets give the ratio of the magnitude of this shift to the FWHM of the resonance in parts per thousand.

	$\Omega_2 T = \frac{\pi}{4}$		$\Omega_2 T = \pi$		$\Omega_2 T = 4\pi$
T/τ	$Sh^{(00)}$	$Sh^{(22)}$	$Sh^{(00)}$	$Sh^{(22)}$	$Sh^{(00)}$
0.2	−290[4.8]	0.11[0.002]	−310[5.1]	2.2[0.054]	−3600[17]
0.5	−50[2.1]	0.044[0.002]	−53[2.1]	0.89[0.054]	−620[7.6]
1	−14[1.2]	0.023[0.003]	−15[1.2]	0.47[0.056]	−170[4.1]
2	−4.3[0.66]	0.013[0.003]	−4.7[0.71]	0.26[0.059]	−50[2.5]
5	−1.3[0.42]	0.007[0.003]	−1.4[0.44]	0.15[0.068]	−10[1.2]
10	−0.81[0.39]	0.006[0.004]	−0.91[0.40]	0.13[0.072]	−3.9[0.75]
20	−0.67[0.37]	0.004[0.003]	−0.71[0.37]	0.067[.037]	−1.8[0.51]
50	−0.60[0.35]	0.002[0.001]	−0.62[0.36]	0.027[0.016]	−0.93[0.39]
100	−0.58[0.34]	0.001[0.001]	−0.59[0.35]	0.014[0.008]	−0.72[0.36]

is being measured ($Sh^{(00)}$ in the table). The values within each row also show that there is a strong dependence on the intensity of the applied field, even though the usual ac Stark shift has already been subtracted out. The additional power-dependent shifts need to be correctly accounted for in precision measurements and will affect extrapolations to zero power for such measurements. Significant shifts still remain from quantum-mechanical interference ($\gamma_{23\to 0} \neq 0$) even in the limit of zero power, and these shifts must also be accounted for in precision measurements. Beside each shift in Table I, the ratio of the magnitude of the shift to the FWHM of that resonance is listed (in parts per thousand) in square brackets. Given that current measurement accuracy for the helium $2\,^3S$-to-$2\,^3P$ intervals is 0.2 parts per thousand of the natural width, the values listed in square brackets in the table are of concern for these measurements [8]. The ratio is larger for the cases of small T or large Ω_2, where the FWHM is also broader than the $\gamma_2/2\pi = 1.6$-MHz natural width.

Although the measurement scheme shown in Fig. 5 is a reasonable and viable method for measuring the $2\,^3S_1$-to-$2\,^3P_1$ interval, the actual measurements of the $2\,^3S$-to-$2\,^3P$ intervals performed to date use more complicated schemes that involve all 12 states shown in Fig. 5. While this paper gives an estimate (based on analytic expressions) for the magnitude of the shifts that will be present in these measurements, an analysis of the correct shift for a particular experiment will require a full numerical calculation based on the density-matrix equations [an expanded set of equations similar to Eqs. (1a)–(1f)], which correctly incorporates the details (laser polarization, laser intensity profile, timing, detection technique, etc.) for the particular measurement.

VI. CONCLUSIONS

In the present paper, we calculated shifts due to quantum-mechanical interference from a distant neighboring resonance. This paper extended the analytic formulas for the simplest three-level system [6] to a more relevant four-level system that included a dark state. In this extended system, the shifts depended on the type of experiment performed (in particular, on which state population was monitored). The shifts for this system can be much larger than those for the simpler three-level system. These interference shifts have been widely overlooked by the atomic-physics precision measurements community. As illustrated for the helium $2\,^3S$-to-$2\,^3P$ intervals, the shifts are large enough to be of concern and need to be carefully considered for precision measurements.

[1] D. A. Cardimona, M. G. Raymer, and C. R. Stroud Jr., J. Phys. B **15**, 55 (1982).

[2] D. A. Cardimona and C. R. Stroud, Phys. Rev. A **27**, 2456 (1983).

[3] S. Haroche, in *Topics in Applied Physics*, edited by K. Shimoda, Chap. 7, Vol. 13 (Springer-Verlag, Berlin, 1976), pp. 253–313.

[4] Z. Ficek and S. Swain, *Quantum Interference and Coherence* (Springer-Verlag, Berlin, 2005).

[5] C. J. Sansonetti, C. E. Simien, J. D. Gillaspy, J. N. Tan, S. M. Brewer, R. C. Brown, S. Wu, and J. V. Porto, Phys. Rev. Lett. **107**, 023001 (2011).

[6] M. Horbatsch and E. A. Hessels, Phys. Rev. A **82**, 052519 (2010).

[7] P. C. Pastor, G. Giusfredi, P. De Natale, G. Hagel, C. de Mauro, and M. Inguscio, Phys. Rev. Lett. **92**, 023001 (2004).

[8] M. Smiciklas and D. Shiner, Phys. Rev. Lett. **105**, 123001 (2010).

[9] J. S. Borbely, M. C. George, L. D. Lombardi, M. Weel, D. W. Fitzakerley, and E. A. Hessels, Phys. Rev. A **79**, 060503 (2009).

[10] T. Zelevinsky, D. Farkas, and G. Gabrielse, Phys. Rev. Lett. **95**, 203001 (2005).

[11] J. Castillega, D. Livingston, A. Sanders, and D. Shiner, Phys. Rev. Lett. **84**, 4321 (2000).

[12] C. H. Storry, M. C. George, and E. A. Hessels, Phys. Rev. Lett. **84**, 3274 (2000).